may be possible to distinguish different contamination sources via their $\delta^{53}Cr$ values.

Our measured groundwater $\delta^{53}Cr$ values (Table 2) ranged from 1.1 to 5.8‰ in the samples from the California site, and from 1.3 to 4.0‰ in the samples from the Connecticut site. All of the groundwater Cr(VI) analyses show enrichment in the heavy isotope relative to the plating baths. Apparently, Cr(VI) reduction has preferentially removed lighter isotopes from the groundwater. The variation in $\delta^{53}Cr$ values at each site suggests that reduction of Cr(VI) is occurring and has progressed to different degrees in different parts of the contaminant plumes. The highest $\delta^{53}Cr$ values are found in the samples with lowest Cr(VI) concentration at both sites. This result is expected because the fringe areas of the contaminant plumes likely have greater degrees of reduction than the plume cores, where Cr concentrations are high and the reducing power of the aquifer materials has been depleted.

Stable Cr isotope ratios can thus serve as indicators of the extent of Cr(VI) reduction in groundwater. For example, if we assume an α value of 0.9966 and a value of 0.34‰ (the mean of the plating bath analyses) for the initial $\delta^{53}Cr$ of the contaminant Cr, we can use Eq. 1 to determine the extent of reduction for two of the Connecticut groundwater samples, MW-9 and MW-12; for these samples, 31% and 68% of the Cr(VI) initially present in the wells was reduced, respectively.

Cr(VI) reduction by bacteria or reducing agents other than those studied here could induce greater or lesser isotopic fractionation than we observed. Processes other than reduction, such as sorption, precipitation, and uptake by plants and algae, can remove Cr from solution (*1, 21–23*). If these processes and/or Cr(III) oxidation induce isotopic fractionation, this could complicate the interpretation of $\delta^{53}Cr$ measurements. However, as with S and Se isotopes (*12*), we expect that the dominant cause of Cr isotope fractionation is oxyanion reduction. Cr isotope studies may also be useful in assessing redox conditions in modern or ancient oceans.

Table 2. Cr isotope ratio determinations.

Sample	[Cr(VI)] (mg/liter)	$\delta^{53}Cr$ (‰)
Reagent Cr, rocks		
$K_2Cr_2O_7$ reagent	—	0.35
$Cr(NO_3)^{2-}$ reagent	—	0.32
BIR basalt (Iceland)	—	−0.04
BHVO basalt (Kilauea)	—	0.05
JB basalt (Japan)	—	−0.04
Plating bath	~10^5	0.37
Connecticut site		
Plating bath 1	~10^5	0.36
Plating bath 2	~10^5	0.29
CrO_3 supply	—	−0.07
MW-8 groundwater	4.5	2.23
MW-9 groundwater	8.61	1.28
MW-11s groundwater	16.1	1.93
MW-11 groundwater	0.63	3.62
MW-12 groundwater	1.63	3.96
California site		
MW-3 groundwater	0.98	1.08
MW-10 groundwater	0.13	5.79
MW-12 groundwater	3.1	3.39

References and Notes

1. R. J. Bartlett, B. R. James, in *Chromium in the Natural and Human Environments*, J. O. Nriagu, E. Niebor, Eds. (Wiley, New York, 1988), pp. 267–304.
2. J. Robles-Camacho, M. A. Armienta, *J. Geochem. Explor.* **68**, 167 (2000).
3. A. Kortenkamp *et al*., *Arch. Biochem. Biophys.* **329**, 199 (1996).
4. S. Loyaux-Lawniczak, P. Lecomte, J.-J. Ehrhardt, *Environ. Sci. Technol.* **35**, 1350 (2001).
5. D. W. Blowes, C. J. Ptacek, J. L. Jambor, *Environ. Sci. Technol.* **31**, 3348 (1997).
6. C. M. Lytle *et al*., *Environ. Sci. Technol.* **32**, 3087 (1998).
7. I. J. Buerge, S. J. Hug, *Environ. Sci. Technol.* **32**, 2092 (1998).
8. P. R. Wittbrodt, C. D. Palmer, *Environ. Sci. Technol.* **30**, 2470 (1996).
9. J. Hoefs, *Stable Isotope Geochemistry* (Springer-Verlag, New York, ed. 3, 1987).
10. J. Boettcher, O. Strebel, S. Voerkelius, H. L. Schmidt, *J. Hydrol.* **114**, 413 (1990).
11. H. G. Thode, J. Monster, in *Fluids in Subsurface Environments—a Symposium* (American Association of Petroleum Geologists, Tulsa, OK, 1965), pp. 367–377.
12. T. M. Johnson, M. J. Herbel, T. D. Bullen, P. T. Zawislanski, *Geochim. Cosmochim. Acta* **63**, 2775 (1999).
13. M. Rotaru, J. L. Birck, C. J. Allegre, *Nature* **358**, 465 (1992).
14. This method is fundamentally different from that used to measure radiogenic ^{53}Cr variations that occur in ancient meteorites. Radiogenic variations in $^{53}Cr/^{52}Cr$ occur in some meteorites as a result of ^{53}Mn decay during the early history of the solar system, but essentially all Earth materials have identical radiogenic contents (*24*). Specifically, we determine variations in the $^{53}Cr/^{52}Cr$ ratio (*15*) and express results as per mil deviations from a standard: $\delta^{53}Cr$ (‰) = $[(^{53}Cr/^{52}Cr)_{sam} - (^{53}Cr/^{52}Cr)_{std}]/(^{53}Cr/^{52}Cr)_{std} \times 1000$, where sam and std refer to sample and National Institute of Standards and Technology Standard Reference Material 979, respectively. External measurement precision is ±0.2‰.
15. Supplementary details of experimental procedures and mass spectrometry are available on *Science* Online at www.sciencemag.org/cgi/content/full/295/5562/2060/DC1.
16. L. D. Anderson, D. B. Kent, J. A. Davis, *Environ. Sci. Technol.* **28**, 178 (1994).
17. Groundwater samples were taken according to EPA protocols (*25*).
18. R. Makdisi, in *Second International Conference on Remediation of Chlorinated and Recalcitrant Compounds, Monterey, CA*, G. B. Wickramanayake, A. R. Gavaskar, M. E. Kelley, Eds. (KelleyBattelle, Columbus, Ohio, 2000), pp. 185–192.
19. K. Govindaraju, special issue, *Geostand. Newsl.* **13** (1989).
20. Roasting of chromite ore to recover Cr should not significantly fractionate Cr isotopes because fractionation is minimal at high temperatures. Subsequent purification steps at lower temperatures may have the potential to fractionate isotopes, but unless there are large losses of Cr, little overall fractionation results (by mass balance).
21. B. R. James, R. J. Bartlett, *J. Environ. Qual.* **13**, 67 (1984).
22. E. E. Cary, Ed., *Chromium in Air, Soil, and Natural Waters* (Elsevier Biomedical, Amsterdam, 1982).
23. B. R. James, R. J. Bartlett, *J. Environ. Qual.* **12**, 177 (1983).
24. A. Shukolyukov, G. W. Lugmair, *Science* **282**, 927 (1998).
25. *SW-846 Test Methods for Evaluating Solid Waste, Physical/Chemical Methods* (U.S. Environmental Protection Agency, Washington, DC, 1992).

26. Supported by NSF grant EAR 00-01153. Initial work was supported by Geological Society of America graduate student grant 6421-99. We thank N. Nikolaidis and L. Hellerich (University of Connecticut), J. Miller (National Chromium), and R. Makdisi (Stellar Environmental Solutions) for groundwater and plating bath samples, and D. Schrag, C. Bethke, and C. Lundstrom for comments.

26 November 2001; accepted 28 January 2002

Mammalian Dispersal at the Paleocene/Eocene Boundary

Gabriel J. Bowen,[1]* William C. Clyde,[2] Paul L. Koch,[1] Suyin Ting,[3,4] John Alroy,[5] Takehisa Tsubamoto,[6] Yuanqing Wang,[4] Yuan Wang[4]

A profound faunal reorganization occurred near the Paleocene/Eocene boundary, when several groups of mammals abruptly appeared on the Holarctic continents. To test the hypothesis that this event featured the dispersal of groups from Asia to North America and Europe, we used isotope stratigraphy, magnetostratigraphy, and quantitative biochronology to constrain the relative age of important Asian faunas. The extinct family Hyaenodontidae appeared in Asia before it did so in North America, and the modern orders Primates, Artiodactyla, and Perissodactyla first appeared in Asia at or before the Paleocene/Eocene boundary. These results are consistent with Asia being a center for early mammalian origination.

Most modern groups of mammals first appeared on the Holarctic continents (Asia, Europe, and North America) in the early Paleogene (*1–6*). Phylogenetic hypotheses point to Asia as the center of origin for many groups (*4*), but intercontinental correlation of faunas is poorly constrained. The Paleocene/Eocene (P/E) boundary is marked by a short-lived [~80,000-year (*7*, *8*)] decrease in the $\delta^{13}C$ of marine (*9–11*) and terrestrial carbon (*8*, *12*, *13*) occurring within the lower third of magnetic polarity chron C24r (*7*, *9*). The first known

appearances of the orders Artiodactyla, Primates (sensu stricto), and Perissodactyla and of the family Hyaenodontidae in North America occur within the 10^4 years after the P/E boundary carbon isotope excursion (CIE) (*8*) and represent immigration during a brief interval of global warmth (*1–4*, *14*). Identification of the CIE in European sections has indicated that ordinal and familial first appearances near the P/E boundary on that continent did not predate those in North America (*13*). In Asia, these groups appear during the Gashatan and Bumbanian Asian Land Mammal Ages (ALMAs) (*15*, *16*), traditionally thought to correlate with the late Paleocene Clarkforkian and early Eocene Wasatchian North American Land Mammal Ages, respectively [(*17*), but also see (*6*, *18*)]. Here we identify the CIE within Asian fossil-bearing strata to constrain correlation of North American and Asian faunal sequences and clarify the relative timing of the first appearance of mammalian groups on these two continents.

We analyzed samples from three measured sections within the Lingcha Formation [Hengyang Basin, Hunan Province, China (Fig. 1)]. The Lingcha Formation consists of brick-red to tan sandstones and mudstones. Section 1 (555.4 m thick) and section 2 (16.8 m) are on the south limb of the syncline that defines the Hengyang Basin, whereas section 3 (284.4 m) is on the north. The pantodont *Archaeolambda* ("lower Lingcha fauna"), characteristically allied with Gashatan and older faunas (*15*, *16*), occurs near the midpoint of section 2. A more diverse fauna ("upper Lingcha fauna") is found near the top of sections 1 and 3. This assemblage includes the perissodactyls *Orientolophus hengdongensis* and *Propachynolophus hengyangensis* and the crown-group rodent *Cocomys lingchaensis*, which are allied with the Bumbanian ALMA (*15*).

We obtained paleomagnetic results from 150 samples through the Lingcha Formation (*19*). Unblocking temperatures for most samples ranged from 670° to 690°C, indicating a hematite remanence carrier. The formation contains four distinct polarity intervals, with the upper Lingcha fauna falling in a long reversed zone at the top of the formation (Fig. 2). Given the hypothesized earliest Eocene

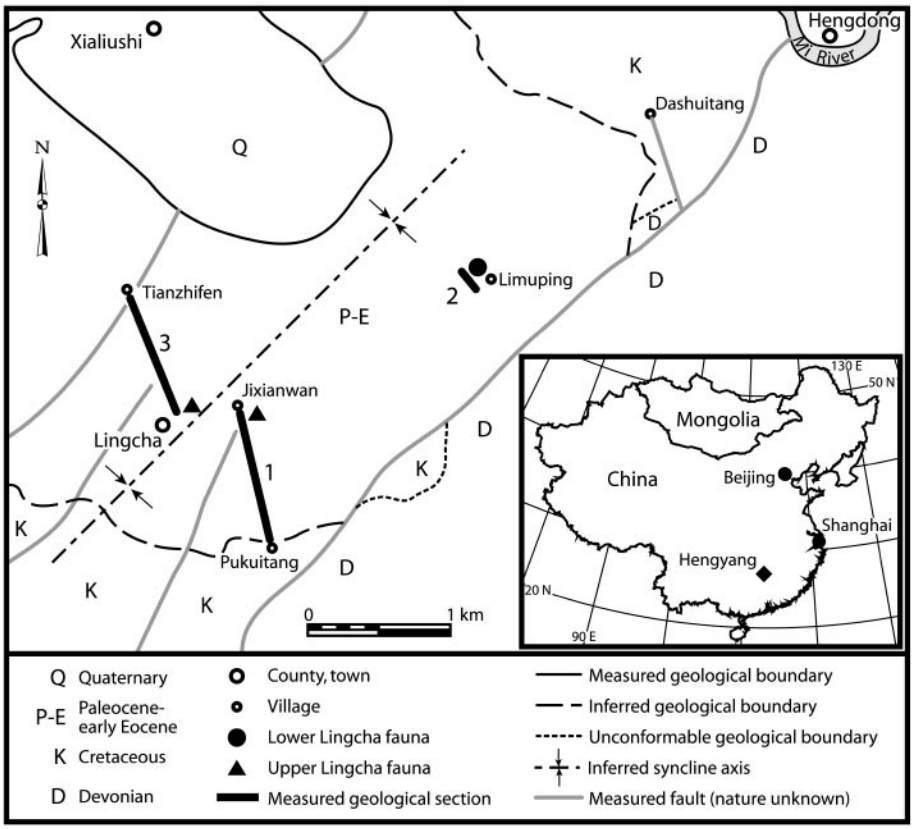

Fig. 1. Geological map of the Hengyang Basin, Hunan Province, China (**inset**). Measured sections 1 through 3 are indicated with bold lines and numbers. Modified from a geological map by the Hengyang Geological Survey.

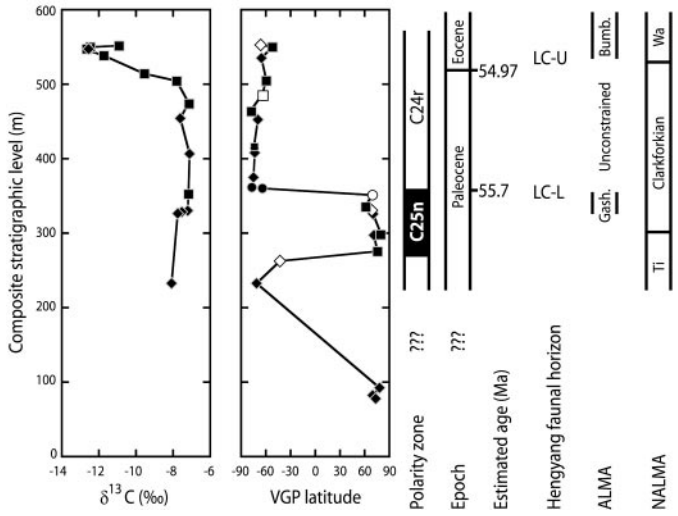

Fig. 2. Carbon isotope and magnetostratigraphy of the P/E transition in the Hengyang Basin, and the proposed intercontinental correlation of late Paleocene/early Eocene mammal faunas. Data from three measured sections, HB-1 (diamonds), HB-2 (circles), and HB-3 (squares), are shown. HB-1 and HB-2 are correlated by trigonometric projection, supported by the magnetic reversal preserved in both sections. HB-1 and HB-3 are correlated based on the presence of a mammal fauna of similar composition and lithologic association preserved near the top of both sections, the low $\delta^{13}C$ values associated with the faunal horizon, and the magnetic reversal ~180 m below the faunal horizon in each section. Isotopic data shown represent average values; the mean $\delta^{13}C$ range for multiple nodules collected at a single stratigraphic level is 0.6‰. VGP, virtual geomagnetic pole. Paleomagnetic data are classed by data quality, where solid symbols are sites with four or more samples significantly grouped at $P < 0.01$, and open symbols represent sites with three or more samples significantly clustered at $P < 0.05$ or two samples significantly clustered at $P < 0.01$. Magnetic polarity zone assignments are based on correlation between terrestrial and marine P/E boundary sections. Ages shown are estimated ages for the chron C25n/C24n boundary (*20*) and the carbon isotope excursion (*25*) (Ma, million years ago). LC-L and LC-U represent the stratigraphic position of the lower and upper Lingcha faunas, respectively. The stratigraphic position of Gashatan (Gash.) and Bumbanian (Bumb.) ALMA is constrained by the LC-L and LC-U faunas, whereas that of the Tiffanian (Ti), Clarkforkian, and Wasatchian (Wa) North American Land Mammal Ages (NALMA) is after Bowen *et al.* (*8*) and Gingerich (*26*).

[1]Department of Earth Sciences, University of California, Santa Cruz, CA 95064, USA. [2]Department of Earth Sciences, University of New Hampshire, Durham, NH 03824–3589, USA. [3]Museum of Natural Science, Louisiana State University, Baton Rouge, LA 70803, USA. [4]Institute of Vertebrate Paleontology and Paleoanthropology, Chinese Academy of Sciences, Post Office Box 643, Beijing 100044, People's Republic of China. [5]National Center for Ecological Analysis and Synthesis, University of California, Santa Barbara, CA 93101–3351, USA. [6]Primate Research Institute, Kyoto University, Inuyama 484–8506, Japan.

*To whom correspondence should be addressed. E-mail: gbowen@es.ucsc.edu

affinities of the upper Lingcha fauna and the Paleocene affinities of *Archaeolambda*, we correlate the uppermost reversed zone to chron C24r (*20*).

The Lingcha Formation includes many discrete horizons with pedogenic carbonate nodules. Previous research has demonstrated that paleosol carbonates can record transient carbon isotope shifts such as the excursion marking the P/E boundary (*12*, *13*). We determined the $\delta^{13}C$ value of 32 nodules from 15 levels within sections 1 and 3 (*19*). Below the 514-m level of our composite section, $\delta^{13}C$ values of paleosol carbonates are consistently between –7 per mil (‰) and –8‰ relative to the Vienna Pee Dee belemnite standard (V-PDB) (Fig. 2). The $\delta^{13}C$ values of carbonate nodules decrease from 514 to 548 m, reaching a minimum of –12.7‰ V-PDB, and then rebound by ~2‰ through the top of the section. The only known shift in the $\delta^{13}C$ of Cenozoic pedogenic carbonate that approximates the magnitude and abruptness of that seen here occurs during the P/E boundary CIE, and we correlate the Hengyang excursion with this event. The stratigraphic position of the Hengyang excursion between mammalian faunas with supposed Paleocene and Eocene affinities and within a long reversed-polarity interval supports this correlation.

The Gashatan lower Lingcha fauna occurs within ~10 m of the chron C25n/C24r reversal; the Bumbanian upper Lingcha fauna occurs near the minimum of the composite $\delta^{13}C$ curve, and in section 1 is directly associated with carbonate nodules with a mean $\delta^{13}C$ value of –12.5‰ V-PDB (Fig. 2). These stratigraphic associations constrain the age of the Gashatan/Bumbanian boundary to between 55.7 and 54.97 million years ago and imply that all Gashatan faunas are of Paleocene age. Perissodactyls, documented in the upper Lingcha fauna, were present in Asia at the P/E boundary, and their Asian first appearance is at least synchronous with their appearance in North America. This result does not offer direct support for the hypothesized Asian origin of this group, but neither does it falsify the hypothesis.

We used appearance event ordination (*19*, *21*, *22*) to correlate Asian faunas traditionally assigned to the Gashatan and Bumbanian ALMAs (Fig. 3). Gashatan and Bumbanian faunas separate unambiguously, firmly supporting the validity of these biochronologic units and supporting our conclusion that all Gashatan faunas are of Paleocene age. Thus, hyaenodontids, which are present in Gashatan faunas in Inner Mongolia [Bayan Ulan fauna (*23*)] and Mongolia [Naran Member, Naran Bulak Formation (*17*)], were present in Asia before they appeared in North America. A perissodactyl has also been reported from Bayan Ulan (*23*), but the species was not recovered during exhaustive resampling of this locality in the 1990s. If this taxon proves to be associated with the Bayan Ulan fauna, it will extend the temporal range of Asian perissodactyls into the Paleocene.

The correlation between most Bumbanian faunas is ambiguous (Fig. 3). The optimal ordination sequence, however, suggests that several Bumbanian faunas may predate the upper Lingcha fauna. Two particularly diverse assemblages, the Wutu fauna and the Bumban fauna, are placed at or near the base of the Bumbanian ALMA. Optimal placement of the Wutu fauna, which includes perissodactyls and artiodactyls, suggests it may be older than other Bumbanian faunas, but our confidence in this correlation is not high (*24*). The Bumban fauna includes perissodactyls and primates, and although its position is better constrained than that of Wutu, the Bumban fauna cannot confidently be assigned a late Paleocene age. Our analysis, then, provides modest support for the hypothesis that perissodactyls, artiodactyls, and primates were present in Asia before their first appearance in North America and Europe during warming at the P/E boundary.

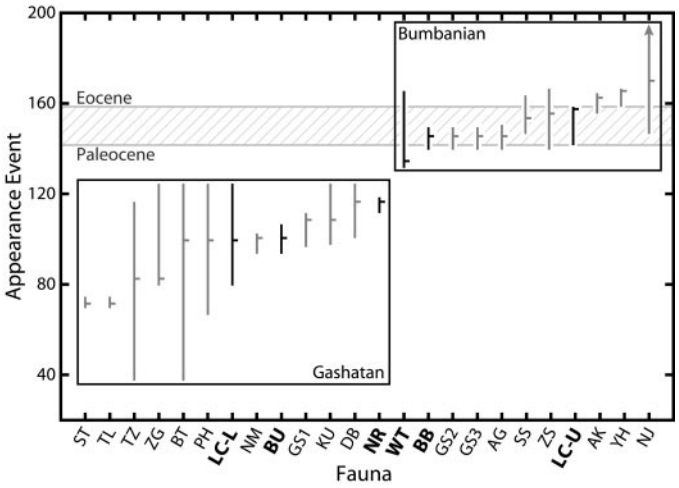

Fig. 3. Appearance event ordination results, based on combined genus- and species-level data, for Gashatan and Bumbanian faunas. Appearance event numbers represent the relative timing of first and last appearance events in the ordered sequence of all events and are a metric of biochronologic time. The biochronologic position of each fauna is constrained by the first and last appearance event numbers of all taxa in the fauna. Horizontal ticks mark the mean position of the optimal range for each fauna, and vertical bars represent the 95% confidence intervals (CIs) on the biochronologic position of faunas, as determined by bootstrapping. Faunas are ordered along the horizontal axis by the mean position of their optimal ranges. Gashatan and Bumbanian faunas are separated unambiguously. The upper Lingcha fauna is correlated to the P/E boundary (Fig. 2), and faunas with 95% CIs that overlap that of LC-U may be either Paleocene or Eocene age (gray diagonal lines). Because the CIs for all Bumbanian faunas intersect this range or are above this range, and no CIs for Gashatan faunas intersect this range, the Gashatan/Bumbanian boundary could be chronologically equivalent to or earlier than the P/E boundary. Faunas discussed in the text (shown with bold text and black symbols) include the following: Naran (NR) and Bumban (BB) Members of the Naran Bulak Formation, Nemegt Basin, Mongolia; Bayan Ulan Formation (BU), Erlian Basin, Inner Mongolia, China; Upper (LC-U) and Lower (LC-L) Lingcha Formation, Hunan, China; and Wutu Formation (WT), Shandong, China. The codes for other Gashatan and Bumbanian faunas (shown with normal text and gray symbols) are given in (*27*).

References and Notes

1. M. C. McKenna, *Ann. MO Bot. Gard.* **70**, 459 (1983).
2. P. D. Gingerich, *Univ. Mich. Pap. Paleontol.* **28**, 1 (1989).
3. D. W. Krause, M. C. Maas, *Geol. Soc. Am. Spec. Pap.* **243**, 71 (1990).
4. K. C. Beard, in *Dawn of the Age of Mammals in Asia*, K. C. Beard, M. R. Dawson, Eds. (Carnegie Museum of Natural History, Pittsburgh, PA, 1998), pp. 5–39.
5. J. J. Hooker, in *Late Paleocene-Early Eocene Climatic and Biotic Events in the Marine and Terrestrial Records*, M.-P. Aubry, S. Lucas, W. A. Berggren, Eds. (Columbia Univ. Press, New York, 1998), pp. 428–450.
6. K. C. Beard, M. R. Dawson, *Bull. Soc. Geol. Fr.* **170**, 697 (1999).
7. U. Röhl, T. J. Bralower, R. D. Norris, G. Wefer, *Geology* **28**, 927 (2000).
8. G. J. Bowen *et al.*, in *Paleocene-Eocene Stratigraphy and Biotic Change in the Bighorn and Clarks Fork Basins, Wyoming*, P. D. Gingerich, Ed. (Univ. of Michigan Museum of Paleontology, Ann Arbor, MI, 2001), pp. 73–88.
9. J. P. Kennett, L. D. Stott, *Nature* **353**, 225 (1991).
10. S. Bains, R. M. Corfield, R. D. Norris, *Science* **285**, 724 (1999).
11. J. Zachos, M. Pagani, L. Sloan, E. Thomas, K. Billups, *Science* **292**, 686 (2001).
12. P. L. Koch, J. C. Zachos, P. D. Gingerich, *Nature* **358**, 319 (1992).
13. I. Cojan, M. G. Moreau, L. E. Stott, *Geology* **28**, 259 (2000).
14. R. B. Peters, L. C. Sloan, *Geology* **28**, 979 (2000).
15. S. Ting, in *Dawn of the Age of Mammals in Asia*, K. C. Beard, M. R. Dawson, Eds. (Carnegie Museum of Natural History, Pittsburgh, PA, 1998), pp. 124–147.
16. Y. Wang, Y. Hu, M. Chow, C. Li, in *Dawn of the Age of Mammals in Asia*, K. C. Beard, M. R. Dawson, Eds. (Carnegie Museum of Natural History, Pittsburgh, PA, 1998), pp. 89–123.
17. D. Dashzeveg, *J. Geol. Soc. London* **145**, 473 (1988).
18. S. G. Lucas, in *Late Paleocene-Early Eocene Climatic and Biotic Events in the Marine and Terrestrial Records*, M.-P. Aubry, S. G. Lucas, W. A. Berggren, Eds. (Columbia Univ. Press, New York, 1998), pp. 451–500.
19. Faunal lists and methods and results for paleomagnetic, isotopic, and biochronologic analyses are available on *Science* Online at www.sciencemag.org/cgi/content/full/295/5562/2062/DC1.
20. S. C. Cande, D. V. Kent, *J. Geophys. Res. Solid Earth* **100**, 6093 (1995).

21. J. Alroy, *Paleobiology* **20**, 191 (1994).
22. _____, *Paleobiology* **26**, 707 (2000).
23. J. Meng, R. Zhai, A. R. Wyss, in *Dawn of the Age of Mammals in Asia*, K. C. Beard, M. R. Dawson, Eds. (Carnegie Museum of Natural History, Pittsburgh, PA, 1998), pp. 148–185.
24. Only one-third of the species from the Wutu assemblage have been described, and the fauna contains a mixture of primitive and derived taxa that leave its position within the ordination poorly constrained.
25. S. L. Wing, H. Bao, P. L. Koch, in *Warm Climates in Earth History*, B. T. Huber, K. G. MacLeod, S. L. Wing, Eds. (Cambridge Univ. Press, Cambridge, 1999), pp. 197–237.
26. P. D. Gingerich, in *Paleocene-Eocene Stratigraphy and Biotic Change in the Bighorn and Clarks Fork Basins, Wyoming*, P. D. Gingerich, Ed. (Univ. of Michigan Museum of Paleontology, Ann Arbor, MI, 2001), pp. 37–71.
27. Other Gashatan and Bumbanian collections represented in Fig. 3 include Zhigden Member (ZG) and Members I (GS1), 2 (GS2), and 3 (GS3) of Khashat Formation, Ulan Nur Basin, Mongolia; Aguyt Member (AG), Naran Bulak Formation, Nemegt Basin, Mongolia; Bugin Member (BT) and Khaychin-Ula 1 fauna (KU), Bugin Tsav Basin, Mongolia; Nomogen Formation (NM), Erlian Basin, Inner Mongolia, China; Taizicun Formation (TZ), Dabu Formation (DB), and Shisanjianfang Formation (SS), Turfan Basin, Xinjiang Region, China; Pinghu Formation (PH), Chijiang Basin, Jiangxi, China; Shuangtasi Formation, Xuancheng Basin (ST), Shuangtasi Formation, Tongling Basin (TL), and Zhangshanji Formation (ZS), Laian Basin, Anhui, China; Yuhuangding Formation (YH), Henan, China; Ningjianshan Member (NJ) of Xinyu Group, Jiangxi, China; and Akasaki Formation (AK), Japan.
28. We thank M. and P. McKenna and S. Xie for assistance in the field and R. Coe for access to the Paleomagnetic Lab at the University of California (UC), Santa Cruz. The paper benefited from discussions with J. Schiebout and J. Meng and from three anonymous reviews. Arrangements and aid in the field were provided by the Institute of Vertebrate Paleontology and Paleoanthropology, Chinese Academy of Science, and the Hengdong County Office, Hunan, China. Funded by National Geographic Society grant 6528-99. G.J.B. was supported by the NSF Graduate Research Fellowship Program, and Y.W. and Y.W. were supported by the Major Basic Research Project of the Ministry of Science and Technology, China (G2000077700). Work by J.A. was conducted while a Center Associate at the National Center for Ecological Analysis and Synthesis, a center funded by NSF (grant DEB-0072909), UC, and UC Santa Barbara. This is Paleobiology Database publication no. 10.

5 December 2001; accepted 29 January 2002

Natural Iron Isotope Variations in Human Blood

Thomas Walczyk[1]* and Friedhelm von Blanckenburg[2]†

Isotopic analysis of human blood and liver and muscle tissue indicates that each individual bears a long-term iron (Fe) isotope signature in the blood. Blood and tissue differ slightly in isotopic composition and are depleted by up to 2.6 per mil in ^{56}Fe relative to ^{54}Fe when compared to dietary Fe. The ^{56}Fe/^{54}Fe isotope ratio in the blood of males is, on average, lower by 0.3 per mil than that of females. These results suggest that Fe isotope effects in the blood reflect differences in intestinal Fe absorption between individuals and genotypes.

Iron (Fe) is essential to the human body for oxygen transport in blood, for oxygen storage in muscle tissue, and as an enzyme cofactor. Iron deficiency anemia (IDA) affects 600 million to 700 million individuals worldwide, and women of childbearing age and children are most vulnerable (*1*). Fe deficiency develops when net Fe losses exceed Fe uptake. Within limits, this can be compensated for by the human body by liberating Fe from the stores in the liver and bone marrow for hemoglobin synthesis. When Fe stores are being depleted, intestinal Fe absorption is increased in parallel (*2*). When stores are empty and up-regulated Fe absorption fails to compensate for Fe losses, the hemoglobin concentration in the blood falls and IDA develops.

Conventional measures of Fe status allow the identification of Fe deficiency and IDA according to population-based reference values. However, because of strong day-to-day variations in Fe absorption, there is no suitable measure to identify whether Fe absorption is up-regulated in the individual to maintain Fe balance or, when Fe supply is abundant, down-regulated to avoid Fe overload.

Here we show that Fe isotope fractionation effects may serve as a tool to identify long-term differences in dietary Fe absorption between individuals. Iron isotope ratios have been commonly measured to study the absorption and utilization of dietary Fe in humans. Such studies use isotopically enriched Fe as tracers (*3*). Sophisticated mass-spectrometric techniques now allow the measurement of small changes in Fe isotope ratios produced by natural processes (*4*). The transport of matter alters the isotopic composition of an element if transfer between reservoirs is incomplete and if the transfer rate is related to the isotope masses. Variations in the ^{56}Fe/^{54}Fe isotope ratio of 1 to 2 per mil (‰) can be induced in natural samples both by microbial activity (*5*) and abiotic processes (*6*, *7*).

Using multicollector inductively coupled plasma mass spectrometry (MC-ICP-MS), we assessed whether the human body discriminates between Fe isotopes and whether Fe isotope effects can be used to trace Fe transport processes in the body. Fe isotopes were analyzed in human blood samples and in liver and muscle tissue and excreta, as well as the main dietary Fe sources of plant and animal origin (*8*).

All blood samples had low Fe isotope ratios relative to the Fe standard of nonbiological origin (Fig. 1). Iron isotope ratios differed by as much as –3.1‰ in the ^{56}Fe/^{54}Fe isotope ratio (δ^{56}Fe) and as much as –4.7‰ in the ^{57}Fe/^{54}Fe isotope ratio (δ^{57}Fe). These are the strongest isotope effects for Fe yet observed in nature. The δ^{56}Fe range in silicate earth is about –0.5‰ to +0.5‰ (*9*), and Fe in bulk soils is relatively uniform at δ^{56}Fe = 0.2‰ (*10*). Model experiments involving Fe-dissimilating bacteria displayed maximum isotope shifts of δ^{56}Fe = –1.3‰ (*5*), and δ^{56}Fe values on the order of –1.6 to 1.0‰ have been found for certain Fe ores (*5*).

All observed isotope shifts are mass dependent (Fig. 1). Our precision (2 SD) of ±0.10‰ for the δ^{56}Fe measurements and ±0.12‰ for the δ^{57}Fe measurements allowed us to resolve differences between individuals. Men and women differed in the Fe isotope composition of their blood (Figs. 1 and 2). Men have a

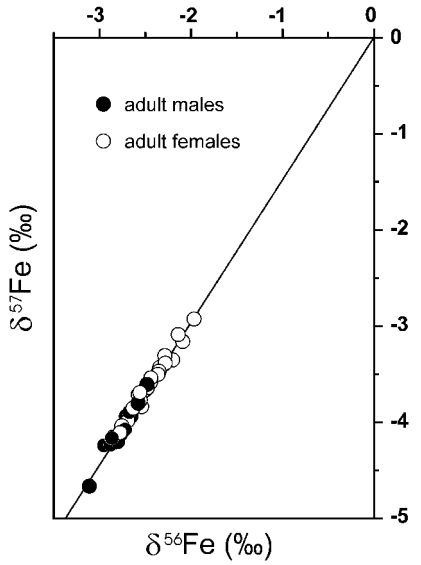

Fig. 1. Fe isotope variations in the blood of apparently healthy human adults. Each point represents an individual person. Data are plotted on a δ scale; that is, as the relative deviation in per mil from the reference isotope ratio (IRM-014, δ = 0). The diagonal line represents the predicted curve for a mass-dependent fractionation process according to an exponential law.

[1]Laboratory of Human Nutrition, Institute of Food Sciences, Swiss Federal Institute of Technology (ETH) Zurich, Seestrasse 72, CH-8803 Rüschlikon, Switzerland. [2]Isotope Geology, University of Berne, Erlachstrasse 9a, CH-3012 Berne, Switzerland.

*To whom correspondence should be adressed. E-mail: thomas.walczyk@ilw.agrl.ethz.ch
†Present address: Institute of Mineralogy, University of Hannover, Callinstrasse 3, D-30167 Hannover, Germany.